10.1109/ULTSYM.2014.0088

Longitudinal monitoring of oxygen saturation with photoacoustic imaging

An early, functional indicator of the *in vivo* efficacy of thermosensitive liposome treatments

Eno Hysi[1], Jonathan P. May[2,*], Lauren A. Wirtzfeld[1], Elijus Undzys[2], Shyh-Dar Li[2,*], Michael C. Kolios[1]

[1]Department of Physics
Ryerson University
Toronto, Canada
mkolios@ryerson.ca

[2]Drug Delivery and Formulation Group
Ontario Institute for Cancer Research
Toronto, Canada
shyh-dar.li@ubc.ca

***Abstract*—Assessing the response of cancer treatments non-invasively on an individual (or patient) basis has the potential to impact cancer treatment. The need for a modality that provides multifaceted information about the structural and metabolic changes that occur within tumors is important, especially because of the vasculature and the role it plays in tumor growth. One such modality capable of imaging the anatomy and functionality of vasculature is photoacoustic (PA) imaging. In this study, *in vivo* PA imaging and estimation of oxygen saturation (SO_2) was performed longitudinally to monitor the efficacy of thermosensitive liposome delivery vehicles. By mapping the distribution of oxygen in 12 animals treated with doxorubicin-loaded thermosensitive liposomes, early SO_2 changes (within hours) were predictive of treatment success as assessed by volumetric tumor growth after 2 weeks. Twelve saline-treated animals showed no observable, early changes in SO_2 and displayed larger intertumoral variability in oxygen distribution compared to the treated group. The longitudinal variations in estimated tumor oxygenation, particularly in the first 5 hours post treatment, demonstrate the unique sensitivity of PA imaging to monitor these functional changes in tumor vasculature.**

Keywords—photoacoustics; treatment monitoring; oxygen saturation; thermosensitive liposomes;

I. Introduction

Vasculature is an essential component of tumor development, providing the increased oxygen and nutrients required for tumors to grow. The structure of the vasculature is highly heterogeneous and lacks the typical organization found in normal tissue; vessels are often oversized, tortuous and leaky creating irregular blood flow patterns [1]. These differences play a role in the tumor vascular microenvironment which significantly differs from otherwise normal tissue. It is often characterized by regions of decreased oxygenation, increased acidity and increased intracellular pressure [2].

Understanding and evaluating the vasculature and oxygenation within tumors is of critical importance for effective treatment design. Cancer cells far away from a blood vessel are unlikely to be killed by systemic chemotherapy. In addition they can be hypoxic which leads to resistance to radiation therapy [3]. New approaches to tumor treatment have focused on the unique aspects of the tumor vasculature. One approach has been to alter the vasculature to improve the flow and structure of the vessels, with the goal of it resembling native tissue. This "normalization" of the vessels has allowed for the improvement of treatments in various carcinomas [4], [5]. Another approach has been to deliver high doses of drugs to the tumor vasculature using mild hyperthermia-induced drug delivery vehicles [6]–[8].

Current cancer imaging techniques are insufficient in evaluating the effects on the vasculature of such treatment approaches, particularly immediately after treatment. The ability to monitor changes in blood flow, oxygenation and microstructure within a tumor in the post-treatment period would allow for an assessment of the treatment efficacy.

Photoacoustic (PA) imaging, with inherently co-registered ultrasound (US) imaging, has the ability to provide a combination of functional and structural information [9]. PA imaging has attracted a lot of attention for its ability to provide co-registered, anatomical and physiological images of vasculature with optical contrast and ultrasonic resolution [10]. As the technique is non-invasive, rapid and safe, longitudinal measurements could be performed to provide information on the changes within the tumor.

The study presented here utilizes high-frequency PA imaging (40 MHz) to track early, functional changes in a murine footpad tumor model treated with a thermosensitive liposome (TSL) drug delivery vehicle. Tumors were repeatedly imaged over a course of hours to days post treatment and the oxygen saturation (SO_2) was estimated as an indicator of therapeutic effect.

II. Materials and Methods

A. Treatment Protocol

EMT-6 murine mammary carcinoma cells (ATCC, Manassas, VA) were cultured in DMEM with 10% FBS and 1% penicillin/streptomycin before subcutaneously injecting 2×10^5 cells in the left footpad of 24 female Balb/c mice (age 6-8 weeks, ~20 g, Jackson Labs (Bar Harbor, USA)).

* JPM and SDL are now at The University of British Columbia Faculty of Pharmaceutical Sciences, Vancouver, Canada.

Tumors were grown for one week prior to treatment. For each imaging session and drug treatment session, mice were anesthetized using isofluorane. All animal studies were performed according to protocols approved by the Animal Care Committee of the University Health Network (UHN, Toronto, Canada).

Animals were treated either with a unique TSL to deliver doxorubicin (HaT-DOX – **H**yperthermia-**a**ctivated cyto**T**oxic) [7] or saline. Twelve mice each received tail vein injections of HaT-DOX (10 mg/kg) or saline followed by immersing the foot with the tumor in a 43°C water bath for 1 h for delivery vehicle activation.

In order to track tumor growth, relative tumor dimensions and body weight were monitored before and for 30 days after treatment for the HaT-DOX animals and 21 days after treatment for the heated saline control (until tumor size endpoint was reached).

B. Imaging Protocol

Animals were imaged with the VevoLAZR US and PA imaging device (Fujifilm VisualSonics, Toronto, Canada) using a nominal 40 MHz US/PA linear array probe coupled to optical fibers. Animals were laid in a prone position on a heated stage with the leg extended and ultrasound coupling gel applied to the foot. Radio frequency (RF) data were collected from pulse-echo US and PA at 750 nm and 850 nm (30 mJ/pulse). All images were acquired in 3D with 80 planes covering approximately 6 mm range. Each tumor was imaged at six time points: immediately pre-treatment, 30 minutes after the completion of the treatment, 2 hours, 5 hours, 24 hours and 7 days post treatment (30m, 2h, 5h, 24h, and 7d). For every time point and all tumors, co-registered US and PA images were acquired.

C. Data Analysis

The procedure for generating the oxygenation maps and respective histograms from the US/PA data is illustrated in Fig. 1 for a representative 2D imaging plane within a tumor. B-mode US slices were reconstructed from the RF data and used to manually segment the tumor region for 21 consecutive 2D planes spanning the tumor as seen in Fig. 1a. The selected region was the region of interest (ROI) for all corresponding US and PA images. The segmented PA images at 750 nm and 850 nm are shown in Figs. 1b and 1c, respectively. The SO_2 value at each pixel was calculated based on the magnitude of the PA signal acquired at 750 nm and 850 nm according to the equation derived in [11], and averaged with a moving average filter to produce a map of the SO_2 values (Fig. 1d). Histograms of the SO_2 values and the corresponding modes were calculated for each of the 21 planes of data (Fig. 1e) and then averaged to give a result per animal for each time point. The histograms were then averaged for the HaT-DOX treated and heated saline groups and plotted with error bars that represent one standard deviation.

III. RESULTS AND DISCUSSION

The treatment efficacy of HaT-DOX compared to the heated saline control was evaluated by tracking the tumor growth. In Fig. 2, the normalized growth is shown, with 100% being the estimate on the day of treatment. The standard deviation across the 12 animals in the treatment group is displayed as error bars. Until 7d post treatment, the increase in the size estimates of the two groups are comparable. Beyond 7d, the HaT-DOX group exhibited a decrease in volume, while the heated saline group continued to grow until the size of the tumor reached the experiment end-point. The variation in tumor size for the heated saline control group was significantly larger than for the HaT-DOX treated group. This observation suggests that control tumors grew at different rates perhaps due to a heterogeneous distribution of vasculature typically seen in untreated tumors [12]. The treated tumors on the other hand showed a smaller degree of size variation possibly due to a more uniform action of the DOX on the vasculature leading to a shut-off in tumor blood supply [13].

Average SO_2 histograms for each time point are presented in Fig. 3, with the HaT-DOX groups (Fig. 3a) showing an immediate shift to the left (drop) in SO_2 30m post treatment which persists until at least 5h post treatment. A slight recovery toward pre-treatment levels is observed 24h post treatment, with a larger increase in SO_2 values by 7d post treatment. The mode (peak of the histograms) for all time points is summarized in Fig. 3c. Specifically, the immediate drop in SO_2 (~15%) observed for the HaT-DOX persists for the first 5h post treatment before an increase of 20% by 7d compared to pre-treatment. It is worth noting that the uniformity in treatment response for the HaT-DOX that was observed in the caliper measurements is also reflected in the low variance of the SO_2 histograms across the 12 treated animals. However, while the caliper measurements did not show the difference in the treatment group compared to the untreated until 14d, the changes in oxygen consumption by the tumor vasculature were detected 30 minutes after treatment. Mapping the distribution of oxygen within the tumor demonstrates how PA imaging can potentially be used to assess the functionality of tumor vasculature and also acts as an early predictor of treatment outcome.

In comparison, the heated saline control group (Fig. 3b) shows comparable pre-treatment SO_2 distribution to HaT-DOX, but bimodal distributions are measured post treatment. This is likely the result of intertumoral heterogeneity. Similar to the HaT-DOX group, an increase in SO_2 values, 20% above pre-treatment, was observed at 7d post treatment, as assessed by the mode of the histograms. There appears to be a correlation between the functional information that PA imaging provides and the tumor growth rate. A large degree of variation in the oxygen distribution was observed for this group at very early time points. This potentially indicates the tumor size variations that were assessed by caliper measurements 14d post treatment. This finding suggests that the anatomical and physiological information that PA imaging is capable of providing has the potential to monitor tumor response to treatment by probing

the development of the vasculature through oxygenation measurements.

IV. CONCLUSIONS

This paper reports on the longitudinal monitoring of TSL treatments using estimations of tumor oxygenation obtained PA imaging. Results suggest a possible correlation between the efficacy of treatment and a reduced tumor SO_2 as early as 30 minutes post treatment. Monitoring oxygen distribution through the use of histograms provides insights into the functional changes occurring in tumor vasculature as treatment progresses.

ACKNOWLEDGMENT

This research was undertaken, in part, thanks to funding from the Ontario Institute for Cancer Research, the Canadian Institutes of Health Research PoP-I, the Terry Fox Research Institute and the Canada Research Chairs program. The authors would like to acknowledge the technical support provided by Fujifilm VisualSonics.

REFERENCES

[1] R. K. Jain, "Delivery of molecular and cellular medicine to solid tumors," *Adv. Drug Deliv. Rev.*, vol. 64, pp. 353–365, Dec. 2012.

[2] J. Fang, H. Nakamura, and H. Maeda, "The EPR effect: Unique features of tumor blood vessels for drug delivery, factors involved, and limitations and augmentation of the effect," *Adv. Drug Deliv. Rev.*, vol. 63, no. 3, pp. 136–151, Mar. 2011.

[3] J. Folkman, "Fundamental concepts of the angiogenic process," *Curr. Mol. Med.*, vol. 3, no. 7, pp. 643–651, 2003.

[4] V. P. Chauhan, T. Stylianopoulos, J. D. Martin, Z. Popović, O. Chen, W. S. Kamoun, M. G. Bawendi, D. Fukumura, and R. K. Jain, "Normalization of tumour blood vessels improves the delivery of nanomedicines in a size-dependent manner," *Nat. Nanotechnol.*, vol. 7, no. 6, pp. 383–388, Apr. 2012.

[5] R. K. Jain, "An Indirect Way to Tame Cancer," *Sci. Am.*, vol. 310, no. 2, pp. 46–53, 2014.

[6] T. Tagami, M. J. Ernsting, and S.-D. Li, "Efficient tumor regression by a single and low dose treatment with a novel and enhanced formulation of thermosensitive liposomal doxorubicin," *J. Controlled Release*, vol. 152, no. 2, pp. 303–309, Jun. 2011.

[7] J. P. May and S.-D. Li, "Hyperthermia-induced drug targeting," *Expert Opin. Drug Deliv.*, vol. 10, no. 4, pp. 511–527, Apr. 2013.

[8] T. Tagami, W. D. Foltz, M. J. Ernsting, C. M. Lee, I. F. Tannock, J. P. May, and S.-D. Li, "MRI monitoring of intratumoral drug delivery and prediction of the therapeutic effect with a multifunctional thermosensitive liposome," *Biomaterials*, vol. 32, no. 27, pp. 6570–6578, Sep. 2011.

[9] L. V. Wang and S. Hu, "Photoacoustic Tomography: In Vivo Imaging from Organelles to Organs," *Science*, vol. 335, no. 6075, pp. 1458–1462, Mar. 2012.

[10] S. Hu and L. V. Wang, "Photoacoustic imaging and characterization of the microvasculature," *J. Biomed. Opt.*, vol. 15, no. 1, p. 011101, 2010.

[11] X. Wang, X. Xie, G. Ku, L. V. Wang, and G. Stoica, "Noninvasive imaging of hemoglobin concentration and oxygenation in the rat brain using high-resolution photoacoustic tomography," *J. Biomed. Opt.*, vol. 11, no. 2, p. 024015, 2006.

[12] R. K. Jain, "Molecular regulation of vessel maturation," *Nat. Med.*, vol. 9, no. 6, pp. 685–693, Jun. 2003.

[13] Q. Chen, A. Krol, A. Wright, D. Needham, M. W. Dewhirst, and F. Yuan, "Tumor microvascular permeability is a key determinant for antivascular effects of doxorubicin encapsulated in a temperature sensitive liposome," *Int. J. Hyperthermia*, vol. 24, no. 6, pp. 475–482, Jan. 2008.

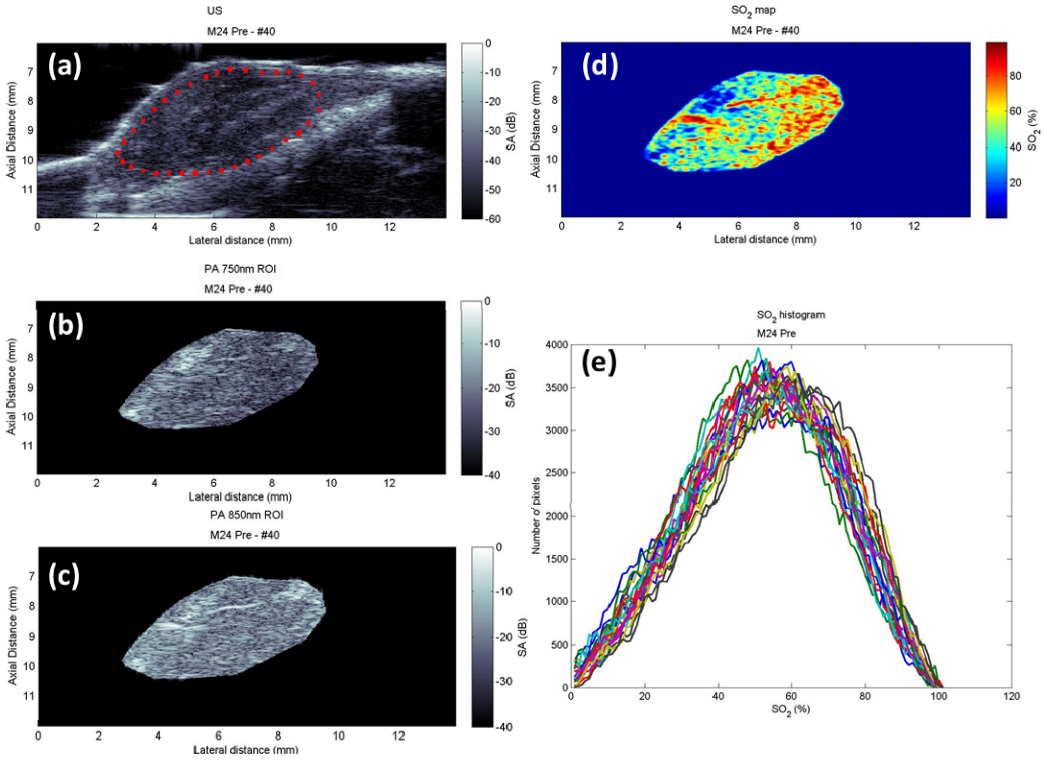

Fig 1: (a) Respresentative US image and ROI selection of a footpad tumor. Corresponding PA image at (b) 750 nm and (c) 850 nm. (d) Oxygen saturation map of the same tumor slice and (e) the corresponding histogram distributions of SO_2 values from 21 tumor slices.

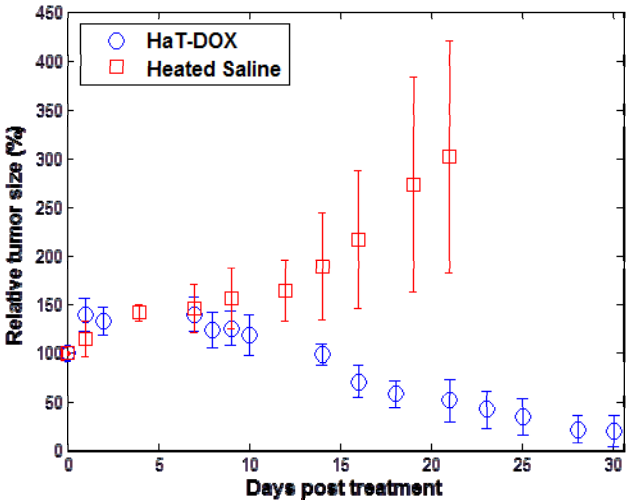

Fig. 2: Treatment efficacy assessed by caliper measurements of tumor sizes as a function of days post treatment. The error bars represent the standard deviations of 12 animals for each treatment group.

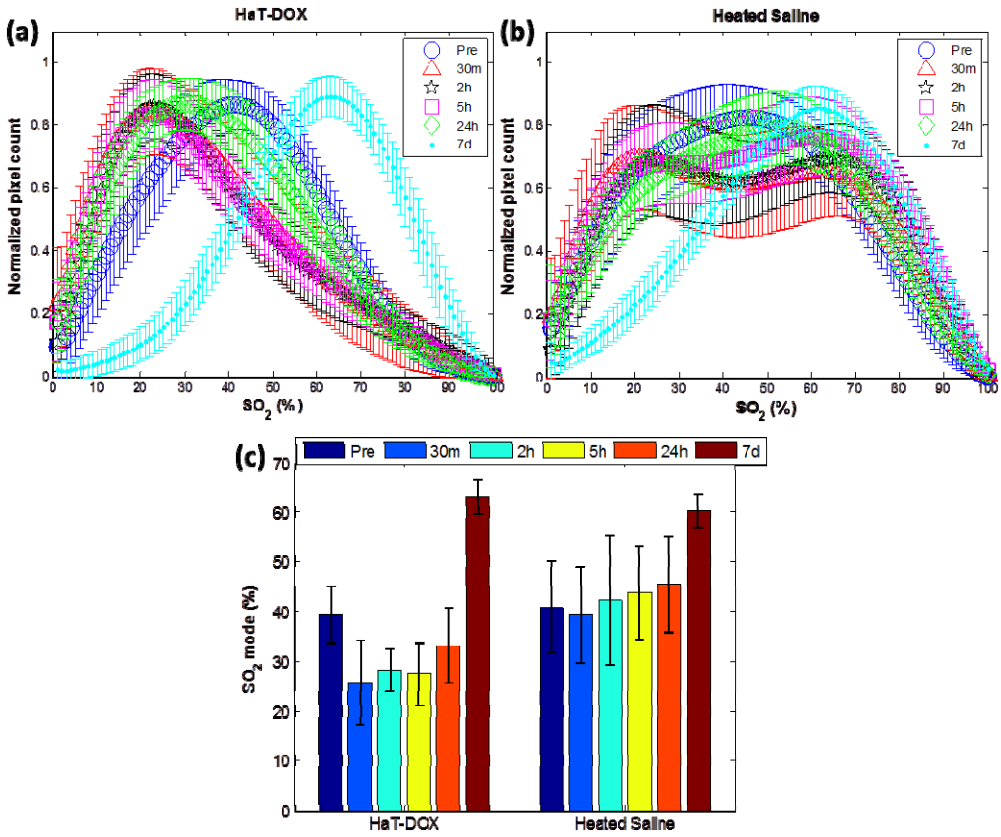

Fig. 3: Average SO_2 histograms and standard deviations for (a) HaT-DOX and (b) saline treated animals. (c) The mode of the SO_2 histograms shown in (a) and (b). The errorbars represent standard deviation of 12 animals per treatment group at each time point.